AMERICAN SOCIETY FOR MICROBIOLOGY | Antimicrobial Agents and Chemotherapy®

MECHANISMS OF ACTION: PHYSIOLOGICAL EFFECTS

Perillyl Alcohol Reduces Parasite Sequestration and Cerebrovascular Dysfunction during Experimental Cerebral Malaria

Adriana A. Marin,[a] Oscar Murillo,[a]* Rodrigo A. Sussmann,[a]* Luana S. Ortolan,[b]* Daniella S. Battagello,[d] Thatyane de Castro Quirino,[c] Jackson C. Bittencourt,[d] Sabrina Epiphanio,[c] Alejandro M. Katzin,[a] Leonardo J. M. Carvalho[e]

[a]Department of Parasitology, Institute of Biomedical Science, University of São Paulo, São Paulo, Brazil
[b]Department of Immunology, Institute of Biomedical Science, University of São Paulo, São Paulo, Brazil
[c]Department of Clinical and Toxicological Analysis, Faculty of Pharmaceutical Sciences, University of São Paulo, São Paulo, Brazil
[d]Department of Anatomy, Institute of Biomedical Science, University of São Paulo, São Paulo, Brazil
[e]Laboratory of Malaria Research, Oswaldo Cruz Institute, Rio de Janeiro, Brazil

ABSTRACT Cerebral malaria (CM) is a severe immune vasculopathy which presents a high mortality rate (15 to 20%), despite the availability of artemisinin-based therapy. More effective immunomodulatory and/or antiparasitic therapies are urgently needed. Experimental cerebral malaria (ECM) in mice is used to elucidate aspects involved in this pathology because it manifests many of the neurological features of CM. In the present study, we evaluated the potential mechanisms involved in the protection afforded by perillyl alcohol (POH) in mouse strains susceptible to CM caused by *Plasmodium berghei* ANKA (PbA) infection through intranasal preventive treatment. Additionally, we evaluated the interaction of POH with the cerebral endothelium using an *in vitro* model of human brain endothelial cells (HBEC). Pharmacokinetic approaches demonstrated constant and prolonged levels of POH in the plasma and brain after a single intranasal dose. Treatment with POH effectively prevented vascular dysfunction. Furthermore, treatment with POH reduced the endothelial cell permeability and PbA parasitized red blood cells in the brain and spleen. Finally, POH treatment decreased the accumulation of macrophages and T and B cells in the spleen and downregulated the expression of endothelial adhesion molecules (ICAM-1, VCAM-1, and CD36) in the brain. POH is a potent monoterpene that prevents cerebrovascular dysfunction *in vivo* and *in vitro*, decreases parasite sequestration, and modulates different processes related to the activation, permeability, and integrity of the blood-brain barrier (BBB), thereby preventing cerebral edema and inflammatory infiltrates.

KEYWORDS *Plasmodium berghei*, experimental cerebral malaria, vascular dysfunction, perillyl alcohol, preventive therapy, immunomodulation

Cerebral malaria (CM) is one of the most serious complications of *Plasmodium falciparum* infection. In regions of endemicity in Africa, CM mostly affects children under the age of five, while in Southeast Asia it is observed mostly in young adults (1). The lethality of CM ranges from 15% to 25% with the best available treatments (2). Over 25% of CM survivors are afflicted with lifelong sequelae, including sensory and cognitive impairment (3). Parenteral artesunate is now widely accepted as the standard of care for the treatment of CM, both in adults and children, following the landmark SEAQUAMAT and AQUAMAT trials that demonstrated its superiority over quinine (4, 5). Nevertheless, treatment with potent artemisinin derivatives alone is insufficient to prevent death or neurological disability in all patients with CM.

Citation Marin AA, Murillo O, Sussmann RA, Ortolan LS, Battagello DS, de Castro Quirino T, Bittencourt JC, Epiphanio S, Katzin AM, Carvalho LJM. 2021. Perillyl alcohol reduces parasite sequestration and cerebrovascular dysfunction during experimental cerebral malaria. Antimicrob Agents Chemother 65:e00004-21. https://doi.org/10.1128/AAC.00004-21.

Address correspondence to Alejandro M. Katzin, amkatzin@icb.usp.br, or Leonardo J. M. Carvalho, leojmc@ioc.fiocruz.br.Tel.

* Present address: Oscar Murillo, University of Texas Health Science Center, Tyler, Texas, USA; Rodrigo A. Sussmann, Institute of Humanities, Arts and Sciences, Federal University of Southern Bahia, Bahia, Brazil; Luana S. Ortolan, Seattle Children's Research Institute, Center for Global and Infectious Diseases Research, Seattle, Washington, USA.

Received 3 January 2021
Accepted 19 February 2021
Accepted manuscript posted online 1 March 2021
Published 19 April 2021

Owing to important limitations in studying the pathogenesis of human cerebral malaria (HCM) and to evaluate novel therapeutic interventions, experimental cerebral malaria (ECM), a neurological syndrome induced in susceptible mice by *Plasmodium berghei* ANKA infection (PbA), has been widely used in pathogenesis and therapeutic investigations since there is evidence that the model shares several features with HCM (6), although important differences are also observed. The pros and cons of this model have been debated elsewhere (7–9). Vascular congestion is a key pathological event in both HCM and ECM, although mechanisms leading to congestion differ. *Plasmodium berghei* does not express orthologues of *Plasmodium falciparum* erythrocyte membrane protein 1 (PfEMP1), whose variants are responsible for *P. falciparum* cytoadherence and sequestration in the brain, a step considered critical in HCM pathogenesis (10). Although receptor-mediated parasitized red blood cells (pRBCs) sequestration may not occur in ECM (11) and leukocyte adhesion to highly inflamed vessels is the key feature observed in this model, accumulation of PbA pRBCs in the brain occurs (12, 13), and the adherent leukocytes can help trap pRBCs (14). A recent elegant study showed that *P. berghei* pRBCs are trapped in cerebral capillaries, likely due to rheological changes of the red blood cells (RBCs), and can block blood flow (15). In addition, trapped pRBCs can focus the damage to endothelial cells and the vessels by providing parasite molecules for endothelial cell activation and antigen presentation to $CD8^+$ T cells, resulting in breakdown of the blood-brain barrier (BBB) and downstream pathogenic mechanisms such as axonal injury (16). Therefore, pRBC accumulation in the brain is also an important step in ECM pathogenesis. Potent proinflammatory responses and increased expression of endothelial adhesion molecules are implicated in parasite or leukocyte sequestration in the cerebral microvasculature and other organs (17). Other factors, such as liver and metabolic alterations, also contribute to ECM pathogenesis (15, 18, 19).

A number of studies have addressed the pathological changes of the BBB in HCM, resulting in increased capillary permeability, cerebral edema, and increased intracranial pressure (20, 21). In ECM, edema is one of the most prominent features of late-stage disease, and widely distributed endothelial cell damage has been reported (22). Mice with ECM show breakdown of the BBB (18, 19, 22), and increased vascular permeability has been described as early as day 3 postinfection in retinal wholemounts (23). Endothelial cells in the microvasculature show signs of damage during the progression of ECM, and $CD8^+$ T cells may impair the function of microvascular endothelial cells via perforin-mediated mechanisms (24). CD8-depleted PbA-infected mice show reduced vascular permeability compared with that of wild-type mice (25). $CD8^+$ T cells are found near sites of pRBC-mediated plugging of small vessels and vascular leakage (16), and $CD8^+$ T cell depletion prevents death by ECM (26). Recently, $CD8^+$ T cells have also been shown to accumulate in the brain in HCM (27, 28). In both ECM and HCM, very low numbers of $CD8^+$ T cells would be enough to mediate vascular damage (16, 26, 27).

Our previous studies have shown that some terpenes, such as nerolidol, limonene, and perillyl alcohol, have inhibitory effects against *P. falciparum* and *P. berghei* growth (29, 30). Mainly, the monoterpene perillyl alcohol (POH) was found to prevent ECM development. This effect, however, did not rely on the antiplasmodial activity, but it was associated with the ability of POH to decrease leukocyte accumulation and hemorrhage in the brains of *P. berghei* ANKA-infected mice and also to downregulate the levels of interleukin 10 (IL-10), IL-6, tumor necrosis factor alpha (TNF-α), gamma interferon (IFN-γ), IL-12, and monocyte chemoattractant protein-1 (MCP-1) in the brain and spleen (31).

In the present study, we further addressed the mechanisms involved in the POH protective effect in ECM by probing whether POH treatment modulates both parasite sequestration in different organs and cerebrovascular inflammation through downregulation of endothelial activation proteins and protection of BBB breakdown. Finally, we

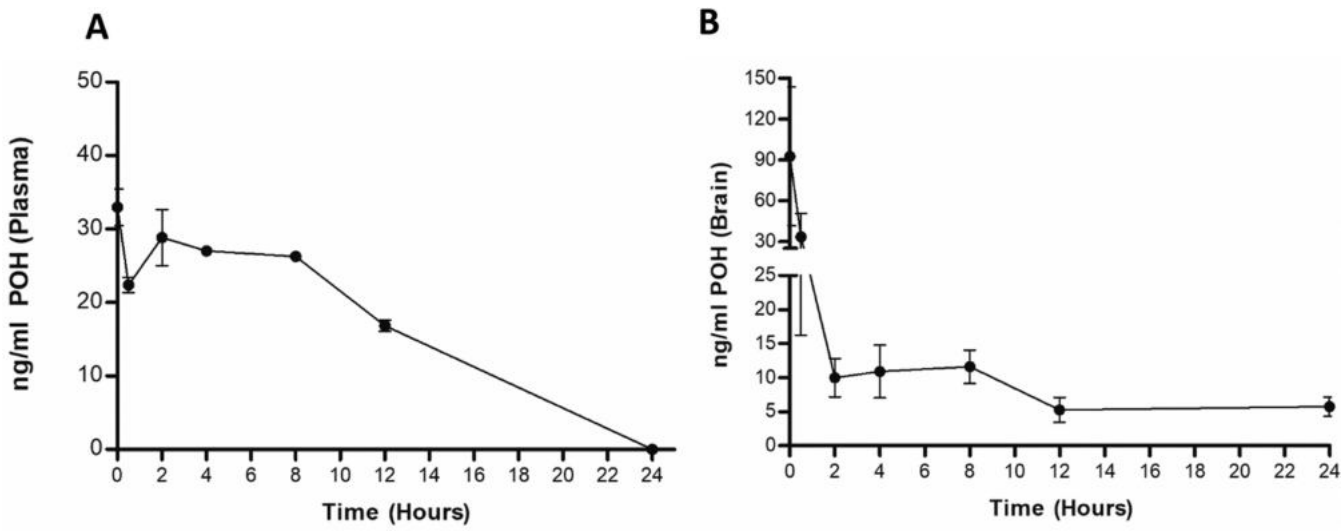

FIG 1 Pharmacokinetic profile of POH in the plasma and brain using GC-MS. C57BL/6 mice were treated with a single dose of 500 mg/kg of POH euthanized at predetermined times ($n = 4$ per group). Plasma and brains were collected, and POH was extracted from the samples and analyzed using GC-MS. (A) Pharmacokinetic profile of POH in the plasma shows that POH remained constant until 8 h after inhalation, the concentration decreased at 12 h, and it was undetected at 24 h after inhalation. (B) Pharmacokinetic profile of POH in the brain shows that the concentration decreased 30 min after inhalation, it remained constant until 12 h, and POH was detected in the brain extracts 24 h after inhalation. Data are presented as mean ± SD.

investigated whether POH affects the cerebral endothelium permeability *in vitro* by evaluating its effect on human brain endothelial cells (HBECs).

RESULTS

Pharmacokinetics of POH in the brain and plasma. The maximum concentration of POH (32.98 ± 4.9 ng/ml) was detected shortly after administration, within 2 min. The concentration of POH in the plasma remained relatively constant until 8 h after inhalation (26.25 ± 0.7 ng/ml), decreased to 16.87 ± 1.5 ng/ml at 12 h, and became undetectable 24 h after inhalation (Fig. 1A). Regarding POH quantification in the brain, we also detected POH until 12 h after a single intranasal dose. Maximal concentration (92.59 ng/ml) after inhalation was detected 2 min after administration. The concentration of POH in the brain decreased substantially 30 min after inhalation (33.47 ng/ml) and then remained constant up to 8 h after inhalation. At 12 h, the concentration decreased further but remained detectable 24 h after inhalation (Fig. 1B). Chromatogram peaks and retention times corresponding to the previously standardized metabolites are shown in Fig. S2.

POH reduces PbA^{luciferase} sequestration in the brain and spleen of PbA-infected mice. POH treatment had no influence on peripheral parasitemia but prevented hypothermia and splenomegaly (Fig. S3). The results presented in Fig. 2 indicate that POH significantly inhibited PbA sequestration. POH-treated mice showed a significant reduction in PbA sequestration in the whole body compared to that of the vehicle-treated mice (Fig. 2A and B). *Ex vivo* images of the organs also confirmed the inhibitory effects. POH prevented PbA sequestration very effectively in the brain and spleen but not in the lungs or the liver (Fig. 2C and D). Reductions in PbA sequestration in the brain and spleen are also reflected in the decrease in the 18S rRNA of the parasite (Fig. 2E).

POH prevents BBB damage in PbA-infected mice. A characteristic feature of inflammation is the breakdown of the BBB. On day 6 postinfection, mice were injected with Evans blue solution to analyze the BBB integrity in uninfected animals and vehicle-treated and POH-treated infected mice. Vehicle-treated PbA-infected mice showed breakdown of the BBB on day 6, with increased leakage of Evans blue into the brain parenchyma. POH treatment prevented leakage, and the levels of Evans blue in the brain parenchyma were not different from those in the uninfected controls (Fig. 3).

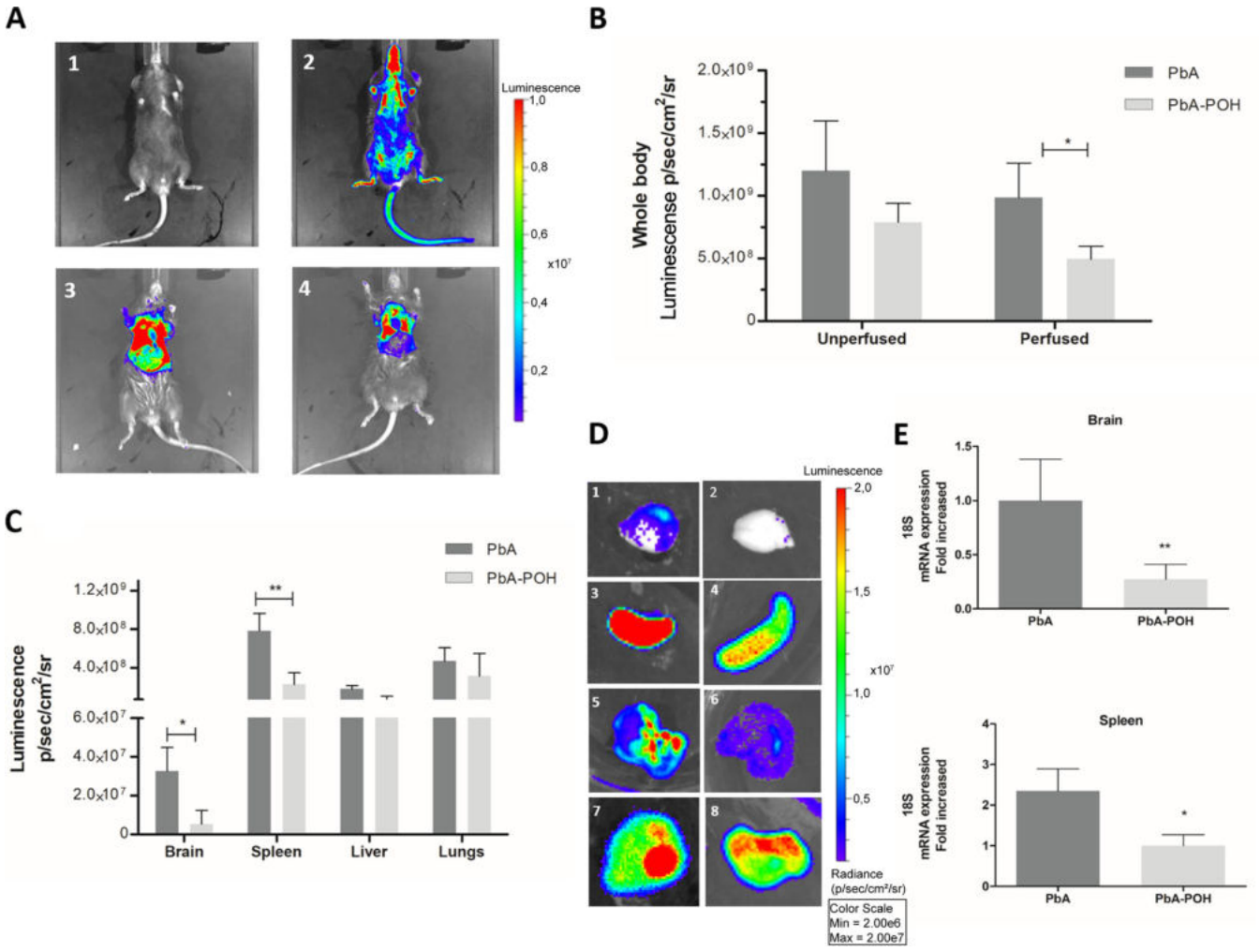

FIG 2 Effect of POH on the PbA luciferase sequestration using bioluminescence. Whole-body imaging after an injection of luciferin from a naive animal (A1), infected, untreated, and unperfused animal (A2), infected, untreated, and perfused animal (A3), and an infected, POH-treated, and perfused animal (A4). (B) Quantification of whole-body bioluminescence of perfused and nonperfused PbA-infected mice treated with POH or vehicle. (C) Quantification of bioluminescence in the brain, spleen, lungs, and liver. (D) *Ex vivo* imaging of the brain, spleen, liver, and lungs of untreated, perfused, and infected animals (D1, 3, 5, and 7) and perfused, infected, and POH-treated animals (D2, 4, 6, and 8). (E) *Plasmodium berghei* 18S RNA levels in the brain and spleen. Data are presented as mean ± standard error of the mean (SEM) ($n = 5$ per group). This figure is representative of data from three independent experiments. *, $P < 0.05$; **, $P < 0.01$; ***, $P < 0.001$.

POH reduces the permeability of HBECs. An *in vitro* cell permeability assay was established using HBEC monolayer (Fig. 4A). Cocultivation of HBECs with *P. falciparum*-parasitized RBCs or with TNF-α (a proinflammatory cytokine closely related to the phenomena of inflammation and endothelial activation) induced marked increases in Evans blue extravasation, indicating loss of cell-cell junction integrity. HBECs stimulated with *P. falciparum* or TNF-α showed a marked increase in interendothelial junctions (OIJs), and these changes were prevented by coincubation with POH (Fig. 4B). Furthermore, the addition of POH substantially prevented Evans blue extravasation in cells stimulated with either *P. falciparum* or TNF-α (Fig. 4C).

POH downregulates ICAM-1, VCAM-1, and CD36 expression in the brains of PbA-infected mice. Damage to the BBB allows leakage of plasma proteins and fluids into the perivascular and parenchymal extracellular spaces, causing vasogenic edema and endothelial activation. Excessive proinflammatory cytokine production leads to cell adhesion receptor upregulation in the brain in ECM, of receptors such as ICAM-1, VCAM-1, and P-selectin. These findings were confirmed in this study. ICAM-1 expression in the mice with ECM showed a 3-fold increase compared with the expression in

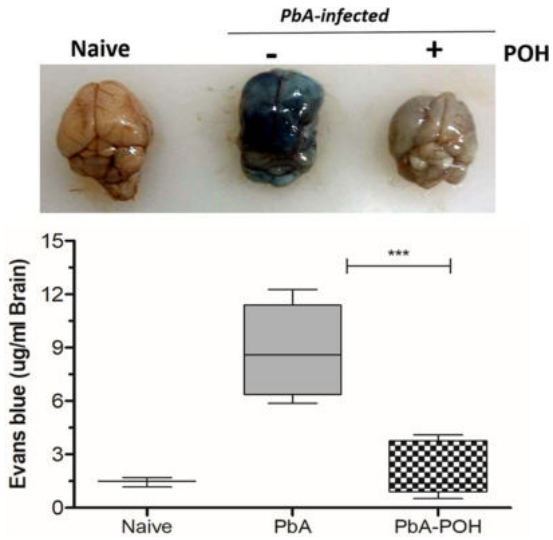

FIG 3 POH prevents the blood-brain barrier breakdown in PbA-infected mice. C57BL/6 mice infected with PbA were treated with 500 mg kg^{-1} day^{-1} POH or vehicle. On day 6 of infection, Evans blue solution was injected intravenously and quantified in the brain. PbA-infected mice showed increased extravasation of Evans blue in the brain, which was prevented by POH treatment ($n = 8$ for POH groups and $n = 3$ for uninfected). The results are shown as mean ± standard deviation (SD). The data are representative of three independent experiments. *, $P < 0.05$; **, $P < 0.01$; ***, $P < 0.001$.

uninfected control mice. POH treatment significantly inhibited the expression of ICAM-1 ($P < 0.01$), VCAM-1, and CD36 ($P < 0.05$) in the brain (Fig. 5A). Indeed, we demonstrated, through immunohistochemistry studies, that ICAM-1 was the endothelial protein most downregulated in the brains of POH-treated mice compared with its expression in PbA-mice. Immunohistochemistry (IHC) profile showed differences between the POH-treated mice and untreated mice. ICAM-1 and VCAM-1 expression was significantly downregulated in POH-treated mice compared to that in PbA-mice. CD36 was the least expressed protein in all the groups; however, it was also downregulated by POH (Fig. 5B and C).

POH reduces $CD4^+$, $CD8^+$, and $CD19^+$ F4/80 cell populations in the spleens of PbA-infected C57BL/6 mice. The results presented in Fig. 6 show the characterization of lymphoid and myeloid populations in the spleens of vehicle-treated and POH-treated mice after 6 days of infection. Vehicle-treated infected mice showed significant increases in the numbers of T ($CD4^+$ and $CD8^+$) and B ($CD19^+$) lymphocytes and macrophages ($F4/80^+$) in the spleen, and POH treatment mostly prevented such increases.

DISCUSSION

The results of POH treatment have demonstrated its high efficacy in preventing parasite accumulation and endothelial dysfunction caused by *P. berghei* infection. POH treatment was effective in preventing parasite sequestration in the spleen and brain. In the brain, we found a marked reduction in *P. berghei* accumulation, probably because of the release of POH via inhalation, since it is known that trigeminal and olfactory nerves can drive drugs directly to the brain, improving its therapeutic potential (32). However, the treatment had a low efficacy in preventing parasite accumulation in the lungs and liver. Until recently, studying the relationship between peripheral blood parasitemia, parasite tissue sequestration, and disease severity has been difficult. Typically, peripheral blood parasitemia is a poor predictor of parasite biomass and disease severity because it only measures circulating immature parasites, not tissue-sequestered mature parasites (33). In this study, POH had little effect on peripheral parasitemia but had a marked effect on parasite accumulation in the brain. In addition, pharmacokinetic approaches demonstrated constant and prolonged levels of POH in the plasma and brain after a single intranasal dose, evidencing that a single daily dose

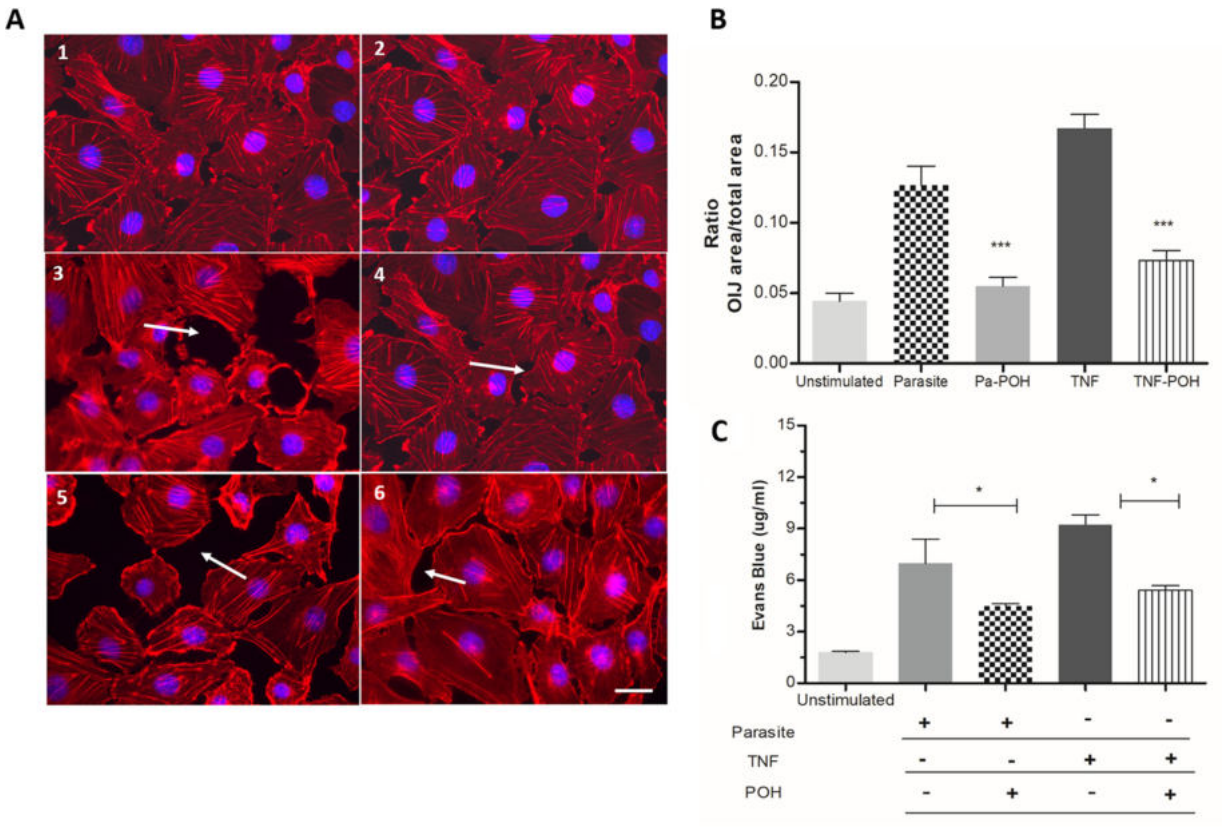

FIG 4 POH decreases endothelial dysfunction in human brain endothelial cells (HBECs). HBECs were stimulated with 50 ng/ml TNF or *P. falciparum*-parasitized red blood cells (at a 30:1 *P. falciparum* to HBEC ratio) and treated with 20 μM POH for 6 h. A range of 10 to 20 pictures of HBECs were taken for each culture using fluorescence microscopy, and representative images were presented for unstimulated cells (A1 to 2), cells stimulated with 30 mature forms of *P. falciparum* per cell (A3), cells stimulated with the parasite and treated with 20 μM POH (A4), cells stimulated with 50 ng/ml of TNF (A5), and cells stimulated with 50 ng/ml TNF and 20 μM POH (A6). White arrows indicate the opening of the interendothelial junctions (OIJs). (B) Data show the ratio of the area of OIJs per total area of each picture. (C) Evans blue leakage was significantly lower in the POH-treated HBECs than in TNF-stimulated and parasite. The results are shown as mean ± SD (scale bars: 50 μm). These graphs are representative of three independent experiments. *, $P < 0.05$; **, $P < 0.01$; ***, $P < 0.001$.

treatment strategy was efficient in guaranteeing the desired therapeutic effect. Reliable and rapid quantification and pharmacokinetics of POH after inhalation delivery are of significant value for the clinic. Extensive pharmacokinetic studies of POH and perillic acid, which is the most abundant metabolite, have been performed after oral delivery of POH (34, 35). Oral delivery of POH at high doses for long periods, however, can result in gastrointestinal toxicity, mainly vomiting and heartburn (36). In contrast, intranasal POH effectively circumvented passage and its associated toxicities were well-tolerated, even after years of continuous use (37).

Prevention of vascular dysfunction by POH treatment was another relevant finding in this study. BBB breakdown is a feature of HCM (21) and ECM (22), causing an increase in vascular permeability and allowing the entry of inflammatory mediators into the brain (17). Proinflammatory cytokine levels were reduced in the brain and spleen of mice with ECM by POH effect (31). In the present study, POH treatment drastically reduced Evans blue leakage in the brains of the treated animals. Additionally, an *in vitro* model using HBECs culture also showed that POH treatment reduced the permeability of endothelial monolayer induced by *P. falciparum* and/or TNF-α. Previous studies have demonstrated a decrease in endothelial tight-junction proteins in both HCM and ECM (38). Damage to the BBB allows leakage of plasma proteins and fluids into the perivascular and parenchymal extracellular spaces, causing vasogenic edema and endothelial activation (38). The upregulation of endothelial receptors is related to severe syndrome during malaria infection (39). ICAM-1 and EPCR expression are

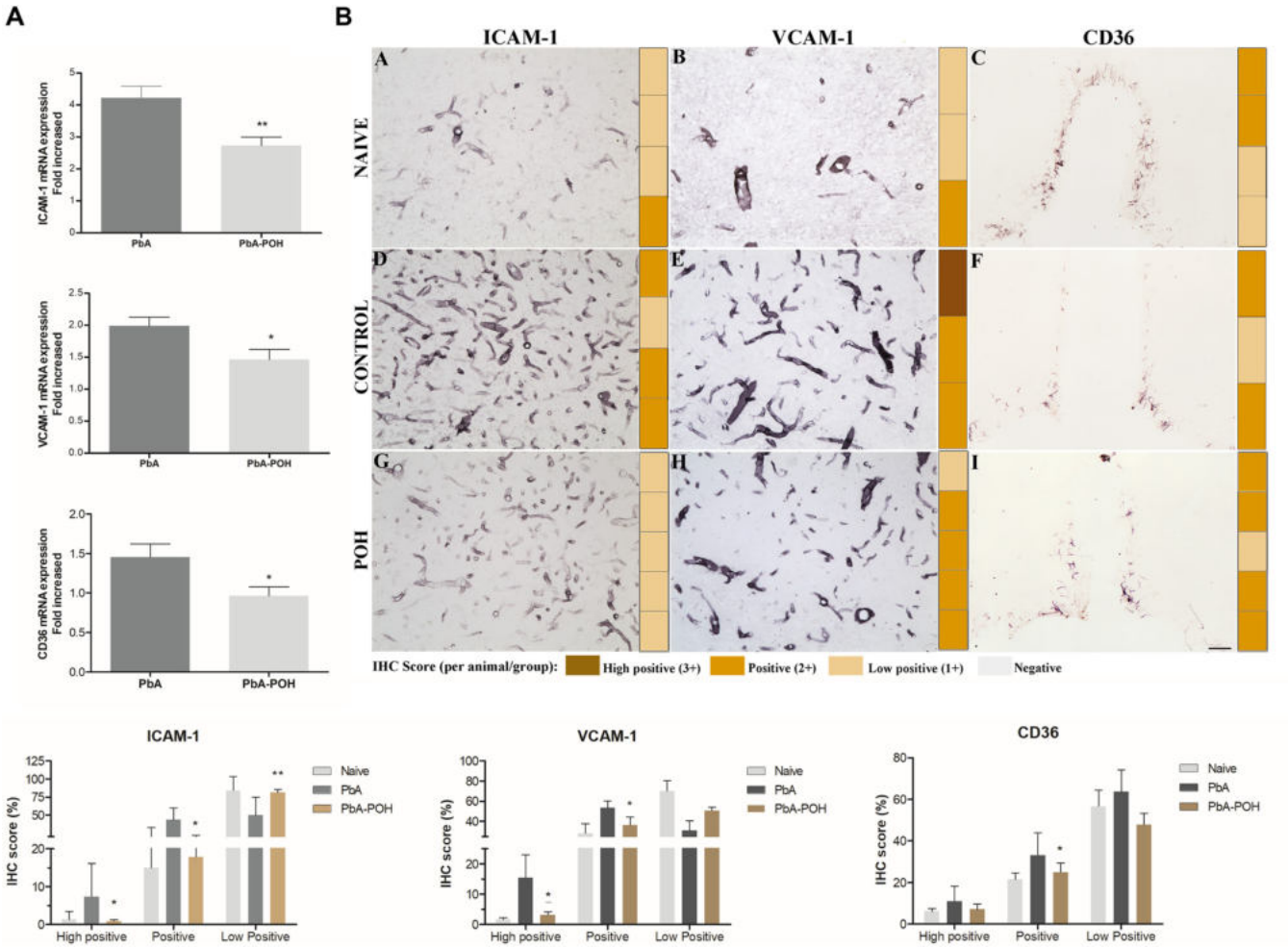

FIG 5 Regulation of ICAM-1, VCAM-1, and CD36 in the brains of PbA-infected mice by POH treatment. C57BL/6 mice were infected with PbA and treated with POH or vehicle ($n = 5$ per group). After 6 days of infection, the brains were removed, processed, and stored until qRT-PCR and immunochemistry analysis. (A) qRT-PCR showed an upregulation of ICAM-1, VCAM-1, and CD36 in untreated PbA-infected mice; POH treatment downregulated the expression of these three adhesion molecules. (B) Representative IHC photomicrographs displaying VCAM-1, ICAM-1, and CD36 immunostaining for all animals/groups. The IHC score (highly positive, positive, low-positive, and negative) for each animal/group ($n = 3$ to 5/group) is represented as a heatmap column on the right side of each representative brightfield photomicrograph. (C) The percentage of IHC score calculated from each staining is represented in graphics for all groups. Taking into consideration the IHC scores analyzed, POH-treated mice showed a lower expression for ICAM-1 and VCAM-1 than did the vehicle-treated mice. Scale bar: 50 μm.

significantly upregulated in the cerebral vascular endothelium in fatal malaria and have been reported as key receptors for *P. falciparum* sequestration in the brains of both adults and children (40–42). In ECM, upregulation of adhesion molecules such as ICAM-1, VCAM-1, and all P-selectins is also observed in the cerebral vascular endothelium of infected mice (17). In addition, ICAM-1-deficient mice do not develop ECM, suggesting that the expression of ICAM-1 is an essential step in severe syndrome development in this model (43). Indeed, previous studies have shown that interventions that decrease the expression of adhesion molecules in the brain, decreasing inflammation and vascular leakage, have beneficial effects in ECM (44, 45), and our findings with POH are in line with such studies. However, it is important to point out that in ECM, vascular adhesion molecule upregulation is not directly related to pRBC sequestration, as it occurs in HCM. Indeed, in HCM, expressed molecules in the brain endothelium such as ICAM-1 and EPCR are directly involved in pRBC sequestration acting as receptors for variants of PfEMP1 (10, 42). *Plasmodium berghei* does not express orthologues of PfEMP1, and its cells are not sequestered through this mechanism. Instead, in ECM, inflammation with endothelial activation and increased expression of adhesion

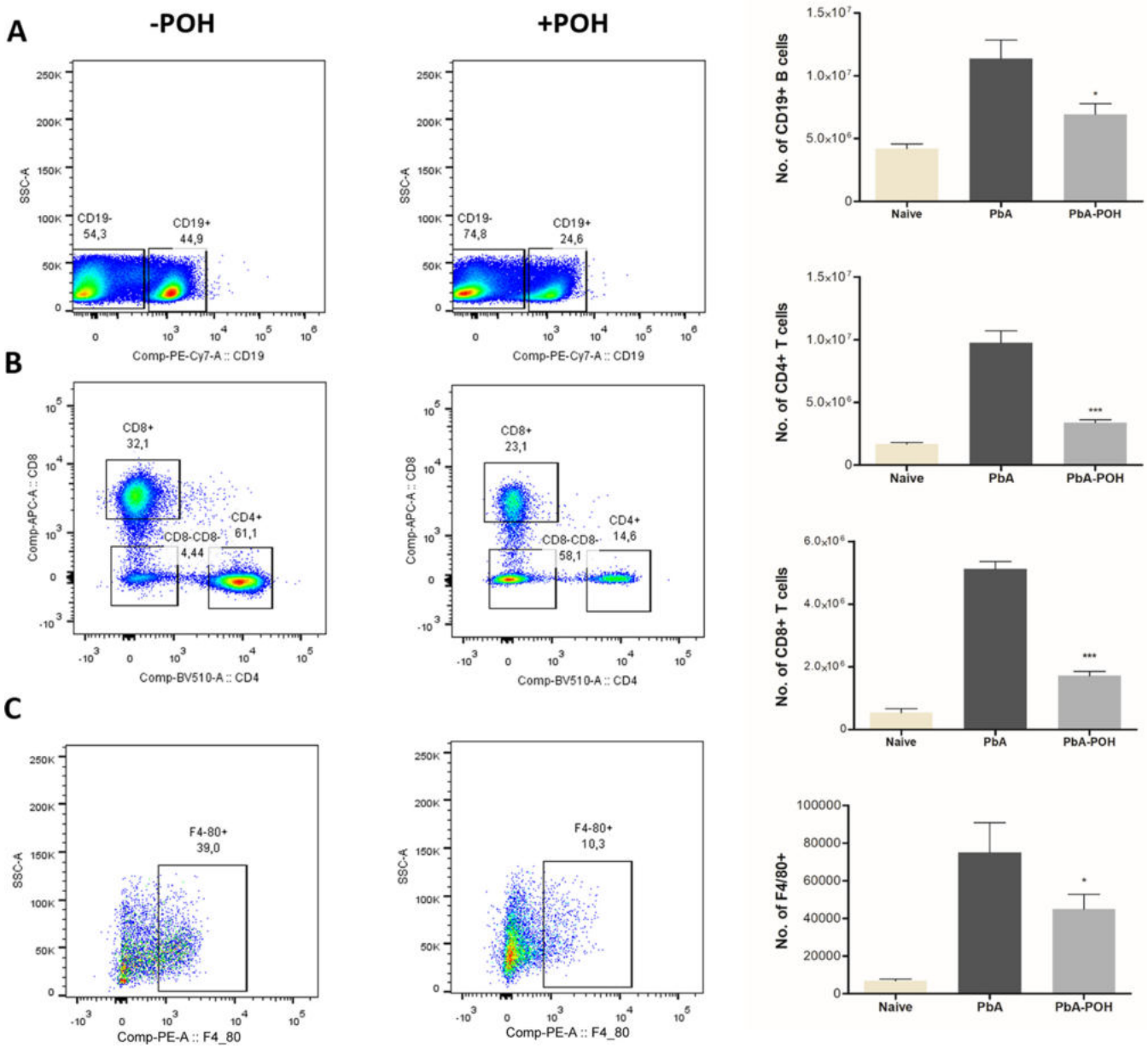

FIG 6 Characterization of lymphoid and myeloid cell populations in the spleen of PbA-infected C57BL/6 mice treated with POH or vehicle after 6 days of infection. The spleen was collected and macerated for total splenocyte isolation. POH showed high efficacy in preventing an increase in T and B lymphocytes and macrophages compared with vehicle. The number of $CD4^+$, $CD8^+$, $CD19^+$, and $F4/80^+$ cells reduced significantly in POH-treated mice. The experiment was repeated twice, and the data represent the mean ± SD ($n = 5$ per group). *, $P < 0.05$; ***, $P < 0,001$.

molecules facilitate leukocyte recruitment and accumulation in brain vessels, resulting in vascular plugging and damage, impaired blood flow, and secondary accumulation of pRBCs (15, 45). In any case, POH-mediated decreased vascular inflammation in ECM helps prevent this leukocyte accumulation, improving cerebral perfusion, which probably could also help in the washout of trapped pRBCs in smaller vessels (16). Among the brain-sequestered leukocytes, $CD8^+$ T cells are present in low numbers in ECM but play a major role in pathogenesis by causing endothelial damage and subsequent collapse of the BBB (26, 46). POH therapy was efficient in controlling the proliferation of $CD8^+$ and $CD4^+$ T cells, B lymphocytes, and macrophage populations in the spleen, and this effect can eventually prevent excessive migration of certain cell types to the brain and therefore decrease local infiltrates. Indeed, the spleen plays a critical role in ECM, as splenectomized mice or mice with irradiated spleens do not develop ECM (47).

Malaria parasites are blood-borne pathogens, and the spleen is the major site for the immune response against them and also where immune cells involved in ECM pathology (e.g., $CD4^+$ and $CD8^+$ T cells) are probably generated and activated. Therefore, POH, by preventing splenic pRBC sequestration and decreasing inflammatory reaction originating in the spleen, will help to prevent ECM. Since sequestration of inflammation-mediated pRBCs and presence of low numbers of effector $CD8^+$ T cells are important factors in HCM pathogenesis (27), POH might also be beneficial in human malaria neurological syndrome.

Extensive literature has reported the chemopreventive and antiproliferative activity of POH against a wide variety of experimental tumors, including lung neoplasms, mammary cancer, and pancreatic and liver tumors, attributable to its ability to effectively inhibit proliferation by inducing cytotoxicity and apoptosis, thereby arresting the cell cycle in the G_0/G_1 phase, and to its anti-inflammatory effects, decreasing systemic cytokine production and consistently inhibiting endothelial P-selectin expression (48–51). Some other mechanisms have also been reported in the literature and are directed with a POH capability to inhibit the prenylation of Ras protein in several types of cell lines (51–54). The membrane anchorage of Ras is facilitated by its prenylation and is required for functional activity in signal transduction which includes a wide variety of cellular processes, including growth, differentiation, cytoskeletal organization, and membrane trafficking (55). Indeed, previous studies have demonstrated that POH was able to inhibit farnesylation proteins in *P. falciparum* (31). In the present study, we have shown the ability of POH to exert an antiproliferative effect in the populations of T and B lymphocytes in the spleen. This effect could be due to the capacity of POH in inhibition or reduction of the prenylation process from these cells. However, this mechanism was not explored in this current approach. Further studies could be addressed in order to deeply examine this mechanism.

The findings in this and our previous study (31) indicate that POH is an efficient monoterpene to prevent ECM development, and its effects are summarized in Fig. 7. POH acts by preventing the overwhelming inflammatory response observed during ECM and preventing splenomegaly and proliferation of macrophage, T cell, and B cell populations, as well as increased cytokine and adhesion molecule expression in the brain, leading to decreased parasite accumulation, BBB breakdown, and tissue damage. The therapeutic potential for POH as an adjunctive therapy administered in combination with an antimalarial drug in the setting of late-stage ECM has not been addressed in this study, and the findings described here may suggest that such trials in the ECM model are worthwhile. On the other hand, POH could be used to decrease inflammatory effects, caused by infectious agents or not, in organs such as brain, spleen, or lungs using this route of administration.

MATERIALS AND METHODS

Mice, parasites, infection, and treatment. Male 6 to 8-week-old C57BL/6 mice weighing 22 ± 2 g each, provided by the Vivarium Sector of the Institute of Biomedical Sciences, University of São Paulo, were kept in rooms with controlled temperature and humidity and a 12 h light/dark cycle. Mice were handled in accordance with the ethical principles of animal experimentation adopted by the Brazilian Society of Laboratory Animal Sciences (approval number 140/2009). *P. berghei* ANKA (PbA) expressing green fluorescent protein (GFP) or luciferase (kindly donated by the Malaria Research and Reference Reagent Resource Center [MR4], Manassas, VA; deposited by C.J. Janse and A.P. Waters; MR4 reagent number MRA-865) was propagated in naive mice. In each experiment, a fresh blood sample was obtained from a passage mouse, and a suspension containing 1×10^6 parasitized red blood cells (pRBCs) in 200 μl was injected intraperitoneally (i.p.) into each experimental mouse. Parasitemia was monitored using flow cytometry and quantified by counting the number of pRBCs in 100,000 RBCs. Clinical assessment was performed according to the previously described methodology (56). Body temperature was monitored by using an Acorn Series Thermocouple thermometer with a mouse rectal probe (Oakton Instruments, Vernon Hills, IL). Mice were treated with 500 mg/kg of POH intranasally (Santa Cruz Biotechnology, Dallas, USA) after 2 h of infection every 24 h for 6 days, and the control group inhaled the vehicle alone (70% ethanol and 10% glycerol) according to a previously described methodology (31).

Determination of POH concentration in the plasma and brain using GC-MS. C57BL/6 mice were treated with a single dose of 500 mg kg^{-1} day^{-1} POH intranasally. Blood and brain samples were collected at predetermined times (0, 0.5, 2, 3, 4, 6, 8, 12, and 24 h). Samples were processed and the

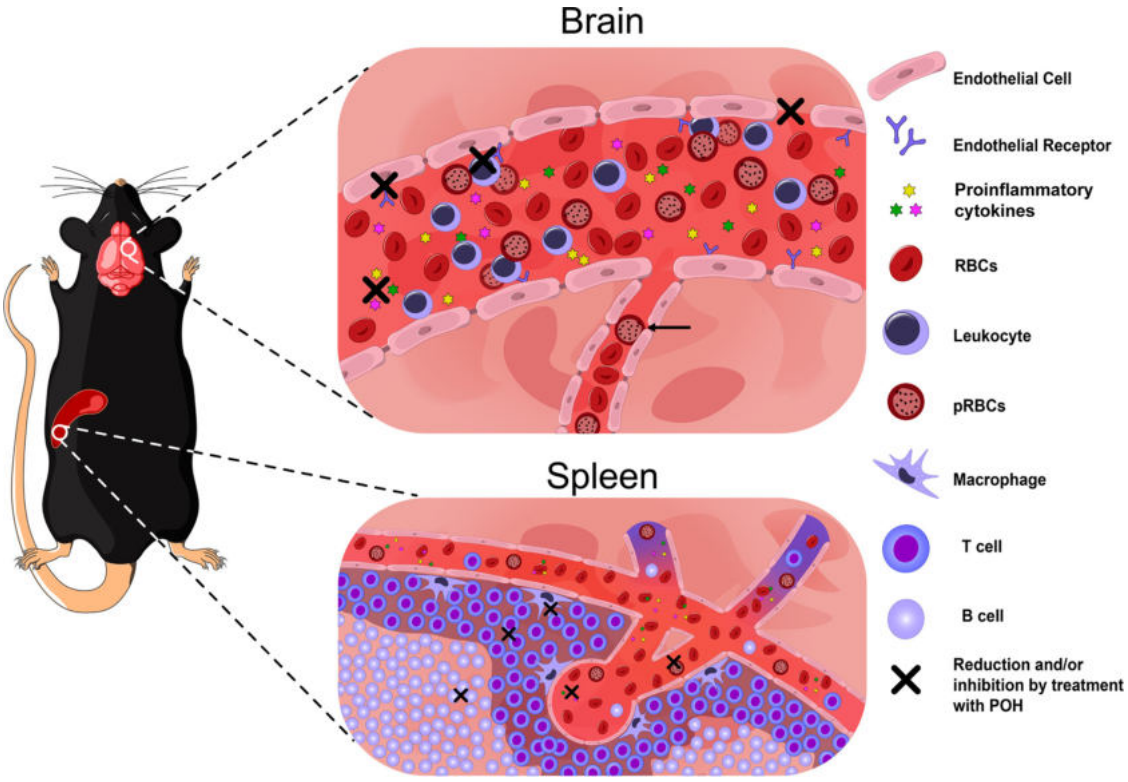

FIG 7 Schematic representation of the mechanism of action of POH as a preventive therapy for experimental cerebral malaria. A 500 mg kg^{-1} day^{-1} dose of POH administered intranasally reduces the cerebrovascular inflammation, preventing leukocyte adhesion and pRBCs accumulation in the larger venules, resulting in decreased vascular congestion. Decreased congestion reduces vascular resistance, and improved blood flow may help to wash out trapped pRBCs in microvessels (black arrow). Also, BBB breakdown was prevented by treatment. In addition, molecules related to endothelial activation, such as ICAM-1, VCAM-1, and CD36, were downregulated by POH. POH treatment led to a significant reduction in T and B lymphocytes and macrophages in the spleen. Therefore, POH effect causes an improvement in neurological and clinical features, preventing ECM development.

supernatant was collected and dried for further gas chromatography mass spectrometry (GC-MS) analysis, as described by Saito et al. (57). For detection of POH and farnesol (internal standard), characteristic ion for both terpenes at *m/z* 93 was monitored by selected ion monitoring (SIM) mode (Fig. S1).

Quantification of *P. berghei* ANKA^{luciferase} sequestration in the brain and other vital organs using bioluminescence. On day 6 postinfection, POH-treated mice and PbA-mice were anesthetized and injected i.p. with D-luciferin substrate (Promises, VivoGlo). After 5 min, the bioluminescence signal of the whole bodies of the animals was monitored through an IVIS Lumina 200 (Xenogen) *in vivo* imaging camera; first without and then after perfusion, the brain and other organs were removed and used for *ex vivo* analysis. The exposure time ranged from 60 to 120 s depending on the signal strength. The mean values of radiation (photons/s/cm^2/sr) were calculated for region of interest (ROI) using Living Image software 4.3.1 (64 bits) for experimental and control animals. Background values were obtained from uninfected mice injected with luciferin.

Assessment of ICAM-1, VCAM-1, and CD36 in the brain using RT-PCR. Studies were conducted on the relative quantification of genes encoding ICAM-1, VCAM-1, and CD36 proteins (Table S1). On day 6 postinfection, POH-treated mice or PbA-mice were anesthetized ($n = 5$ per group) and the brains were removed for RNA extraction using RNEasy Micro kit (Qiagen) extraction kit according to the manufacturer's recommended protocol (for purification of total RNA from animal and human cells). All results were normalized according to the expression of the constitutive hypoxanthine-guanine phosphoribosyl transferase (HPRT) gene and the data were analyzed using the $2^{-\Delta\Delta CT}$ relative quantification method, as described by Livak et al. (58). Gene expression in uninfected animals was used as the baseline parameter. Reverse transcription-quantitative PCR (qRT-PCR) was performed on the 7500 Fast apparatus (Applied Biosystems).

Assessment of ICAM-1, VCAM-1, and CD36 in the brain using immunohistochemistry. On day 6 postinfection, POH-treated mice or PbA-mice ($n = 5$ per group) were anesthetized and perfused transcardially via the ascending aorta with approximately 20 ml of cold 0.9% saline. This step was followed by 250 ml of cold 4% formaldehyde in borate buffer (0.1 M, pH 9.5). The brains were dissected and postfixed in the same fixative solution with 20% sucrose overnight. Next, frontal plane brain slices were obtained in a freezing microtome (SM2000R, Leica, Germany) with 20 μm thickness in five series. The slices were stored in antifreeze solution at −20°C until immunohistochemistry method.

To identify and localize the ICAM-1, VCAM-1, and CD36 immunoreactive cells in all groups, we

performed the indirect immunoperoxidase method. Series of sections were rinsed in 0.02 M potassium phosphate buffer (KPBS, pH 7.4) and pretreated with a solution of 0.3% hydrogen peroxide (H_2O_2) diluted in KPBS for 15 min. Next, the sections were rinsed in KPBS and then incubated in KPBS solution containing 0.03% Triton X-100, 3% normal goat serum (Abcam, USA, AB_2716553), or 3% normal rabbit serum (Vector Laboratories, USA, AB_2336619) with the primary antibody at 1:3,000 overnight at 4°C (Table S2). Afterward, the sections were washed in KPBS and incubated in KPBS solution containing 0.03% Triton X-100 with biotinylated secondary antibody at 1:800 (Abcam, USA, AB_954902 or Vector Laboratories, USA, AB_2336126) for 1 h at room temperature. Next, the slices were washed in KPBS and then incubated in avidin-biotin-horseradish peroxidase solution at 1:333 (Vectastain ABC Elite, Vector Laboratories, AB_2336819) for 1 h at room temperature. After washes in KPBS, the slices were submitted to the peroxidase reaction using a solution of 0.003% hydrogen peroxide, 3,3′-diaminobenzidine tetrahydrochloride (DAB; 0.02%, Sigma Chemical, USA) as a chromogen, and 2.5% nickel ammonium sulfate (NAS; Alfa Aesar, USA) diluted in 0.2 M sodium acetate buffer (pH 6.5) as a reaction amplifier. After washes, sections were mounted onto gelatin-coated glass slides, dehydrated in ascending concentrations of alcohol, deparaffinized in xylene, covered with a hydrophobic mounting medium (DPX, Sigma, USA), and coverslipped.

Brightfield photomicrographs were acquired with a Nikon Eclipse 80i upright microscope (Nikon, Japan) coupled to a digital camera (CX3000) operated with Microlucida 3.03 acquisition software (MicroBrightField Inc., USA). All images were adjusted for brightness and contrast to provide uniformity among the sections to do the analysis using Adobe Photoshop CS5.1 (Adobe Systems Inc., USA). For immunohistochemistry (IHC) quantification, we used a semiquantitative method to represent staining intensity which analyzes IHC photomicrographs using an IHC profiler. This IHC profiler has been well done and accepted in the scientific literature for semiquantitative measurements, with high confidence and accuracy (59–64). We randomly selected areas of the cerebral cortex (VCAM-1/ICAM-1) and periventricular zone of the hypothalamus (CD36) to obtain the individual score labeling for each animal in all groups. The analysis was performed by a researcher blinded to the results. The IHC images obtained from the brain areas were analyzed by IHC profiler plugin using the ImageJ software (65) and by color deconvolution (DAB-stained); therefore, an IHC score was generated for each animal/group based on automated pixel counting (independent scores): 3+ (highly positive), 2+ (positive), 1+ (low-positive), 0 (negative) (64). Each IHC score/animal/group is represented as a heatmap column on the right side of each representative brightfield photomicrograph for each animal/group analyzed. The most frequent score was selected to represent the pattern of staining for VCAM-1, ICAM-1, and CD36 for each group of animals analyzed, based on previous study (63). Moreover, the percentage of IHC score calculated from each staining is represented in graphics for all groups.

Assessment of BBB permeability. BBB integrity was assessed using the Evans blue assay. Briefly, on day 6 postinfection, POH-treated mice and PbA-mice were anesthetized and a 0.2-ml solution of 2% Evans blue (Sigma-Aldrich) in phosphate-buffered saline (PBS) was injected intravenously into each mouse. One hour later, mice were euthanized, the brain was removed, and Evans blue dye was extracted from the brain tissue with 100% formamide (Sigma-Aldrich) for 48 h. The amount of Evans blue per milliliter of brain tissue extracts was determined by measuring the absorbance at 620 nm.

Permeability assay and morphometric analysis of the opening of OIJs of HBECs. Human brain endothelial cells (HBECs/D3 cell line), kindly provided by Julio Scharfstein (Federal University of Rio de Janeiro, Rio de Janeiro, Brazil), were cultured in Dulbecco modified Eagle medium (DMEM) supplemented with 10% fetal bovine serum and gentamicin at 37°C in a 5% CO_2 atmosphere until confluent. The cells were then plated on 24-well transwell plates (Corning) (3×10^5 cells/well) and incubated for 24 h. Mature forms of *P. falciparum*/3D7 strain (unselected for receptor-specific cytoadherence) (30:1) or 50 ng/ml of TNF-α were plated for 6 h, and 20 μM POH was added concomitantly. After 6 h with the different stimuli, 0.1 ml of 1% Evans blue solution was added in each well for 40 min. The amount of Evans blue leakage was determined by measuring the absorbance at 620 nm. In order to identify actin microfilaments and quantify OIJs, we performed the actin immunofluorescence using Texas Red phalloidin. HBECs/D3 line were plated in 24-well plates (3×10^5 cells/well), adhered to gelatin on glass coverslips, and maintained at 37°C with 5% CO_2. The cells were stimulated with mature forms of 3D7 strain of *P. falciparum* (unselected for receptor-specific cytoadherence) and TNF-α for 6 h and cotreated with 20 μM POH. Subsequently, the cells were fixed with 3.7% formaldehyde, permeabilized with acetone at −20°C, and blocked with 1% bovine serum albumin solution. Actin was marked with Texas Red phalloidin (Life Technologies) for 20 min. The cell nuclei were stained with Hoechst (H33342, Life Technologies). Each slide, with fully confluent cells, was chosen randomly and 10 to 20 pictures were taken and scanned in a "zig-zag" way, from top to bottom. The quantification was performed by a researcher blinded to the results. The images were acquired using a fluorescence Axio Imager M2 (Zeiss) microscope using the Axio Cam HRc (Zeiss) and Axio Vision software, version 4.9.1.0. The total area of the OIJs was measured in each picture using the software ImageJ.

Characterization of cellular populations from the spleens of C57BL/6 mice using flow cytometry. On day 6 postinfection, POH-treated mice or PbA-mice were anesthetized, and the spleens were collected and immediately placed in RPMI medium containing 10% fetal bovine serum and cut into pieces. Tissue extracts were macerated with a 100-μm nylon cell filter, and then the cell-free supernatant was centrifuged at $400 \times g$ for 5 min and the pellets were resuspended in RPMI. The cell suspension was treated with RBC lysis buffer (155 mM NH_4Cl, 10 mM $NaHCO_3$, 0.1 mM EDTA [pH 7.3]) to remove RBCs. Cell viability was verified using Trypan Blue (Sigma-Aldrich). The cells (1×10^6 cells per well) were incubated with PerCP-Cy5.5-conjugated anti-CD3 antibody (clone145-2C11, BD Biosciences), PE-Cy7-conjugated anti-CD19 antibody (clone 1D3, BD Biosciences), APC-conjugated anti-CD8 antibody (clone53-6.7,

BD Biosciences), BV510-conjugated anti-CD4 antibody (cloneRM4-5, BD Biosciences), and BV786-conjugated anti-Ly-6G antibody (clone 1, BD Biosciences) for 1 h at 4°C. The cells were washed and suspended in PBS and analyzed using the LSR Fortessa BD cytometer. The results were analyzed using FlowJo X software.

Statistical analysis. For comparison of means of more than two treatments, variables with normal distribution were analyzed using one-way analysis of variance, and other variables were analyzed using nonparametric Kruskal–Wallis tests, with Tukey's or Dunn's posttest. For comparison of means between two groups, an unpaired Student's *t* test was used. The analyses were performed using GraphPad PRISM software version 5.3. *P* values of <0.05 were considered statistically significant.

SUPPLEMENTAL MATERIAL

Supplemental material is available online only.

SUPPLEMENTAL FILE 1, PDF file, 0.6 MB.

ACKNOWLEDGMENTS

We thank the Vivarium Sector of the Institute of Biomedical Sciences, University of São Paulo for providing the animals. Thanks to Danielle Gomes and Juliane Afonso for the support and technical assistance. We thank the Research Support Facilities Center (CEFAP-USP) for the equipment used in this study. We thank Sílvia Beatriz Boscardin and Cláudio Romero Farias Marinho for their discussion and suggestions. The *in vitro* experiments were performed in the laboratory of Cláudio Romero Farias Marinho with technical support from Erika Paula Machado Peixoto. We thank Fernando Sulczewski for helping with cellular characterization using flow cytometry. We also thank Melina Merlone (Fiocruz-Rio de Janeiro) for helping with vascular permeability. This work was supported by grants from Fundação de Amparo à Pesquisa do Estado de São Paulo (FAPESP; grant number 2017/22452-1) Brazil. A.A.M.R., O.M., R.A.S., and L.O. received a postgraduate fellowship from FAPESP. T.C.Q. and D.S.B. were fellowship recipients of the Brazilian Coordenação de Aperfeiçoamento de Pessoal de Nivel Superior (grant PNPD/CAPES, Office for the Advancement of Higher Education). L.J.M.C. received productivity fellowships from Conselho Nacional de Desenvolvimento Científico e Tecnológico (CNPq) and Fundação de Amparo à Pesquisa do Estado de Rio de Janeiro (Faperj – "Cientista do Nosso Estado") and is a member of INCT-NIM-CNPq.

REFERENCES

1. Idro R, Ndiritu M, Ogutu B, Mithwani S, Maitland K, Berkley J, Crawley J, Fegan G, Bauni E, Peshu N, Marsh K, Neville B, Newton C. 2007. Burden, features, and outcome of neurological involvement in acute falciparum malaria in Kenyan children. JAMA 297:2232. https://doi.org/10.1001/jama.297.20.2232.
2. Hochman SE, Madaline TF, Wassmer SC, Mbale E, Choi N, Seydel KB, Whitten RO, Varughese J, Grau GER, Kamiza S, Molyneux ME, Taylor TE, Lee S, Milner DA, Kim K. 2015. Fatal pediatric cerebral malaria is associated with intravascular monocytes and platelets that are increased with HIV coinfection. mBio 6:e01390-15. https://doi.org/10.1128/mBio.01390-15.
3. John CC, Bangirana P, Byarugaba J, Opoka RO, Idro R, Jurek AM, Wu B, Boivin MJ. 2008. Cerebral malaria in children is associated with long-term cognitive impairment. Pediatrics 122:e92–e99. https://doi.org/10.1542/peds.2007-3709.
4. Dondorp AM, Fanello CI, Hendriksen IC, Gomes E, Seni A, Chhaganlal KD, Bojang K, Olaosebikan R, Anunobi N, Maitland K, Kivaya E, Agbenyega T, Nguah SB, Evans J, Gesase S, Kahabuka C, Mtove G, Nadjm B, Deen J, Mwanga-Amumpaire J, Nansumba M, Karema C, Umulisa N, Uwimana A, Mokuolu OA, Adedoyin OT, Johnson WB, Tshefu AK, Onyamboko MA, Sakulthaew T, Ngum WP, Silamut K, Stepniewska K, Woodrow CJ, Bethell D, Wills B, Oneko M, Peto TE, Von Seidlein L, Day NP, White NJ. 2010. Artesunate versus quinine in the treatment of severe falciparum malaria in African children (AQUAMAT): an open-label, randomised trial. Lancet 376:1647–1657. https://doi.org/10.1016/S0140-6736(10)61924-1.
5. SEAQUAMAT group. 2005. Artesunate versus quinine for treatment of severe falciparum malaria: a randomized trial (SEAQUAMAT). Lancet 366:717–725. https://doi.org/10.1016/S0140-6736(05)67176-0.
6. de Souza JB, Hafalla JCR, Riley EM, Couper KN. 2010. Cerebral malaria: why experimental murine models are required to understand the pathogenesis of disease. Parasitol 137:755–772. https://doi.org/10.1017/S0031182009991715.
7. Carvalho LJM. 2010. Murine cerebral malaria: how far from human cerebral malaria? Trends Parasitol 26:271–272. https://doi.org/10.1016/j.pt.2010.03.001.
8. White NJ, Turner GDH, Medana IM, Dondorp AM, Day NPJ. 2010. The murine cerebral malaria phenomenon. Trends Parasitol 26:11–15. https://doi.org/10.1016/j.pt.2009.10.007.
9. Rénia L, Grüner AC, Snounou G. 2010. Cerebral malaria: in praise of epistemes. Trends Parasitol 26:275–277. https://doi.org/10.1016/j.pt.2010.03.005.
10. Baruch DI, Gormely JA, Ma C, Howard RJ, Pasloske BL. 1996. *Plasmodium falciparum* erythrocyte membrane protein 1 is a parasitized erythrocyte receptor for adherence to CD36, thrombospondin, and intercellular adhesion molecule 1. Proc Natl Acad Sci U S A 93:3497–3502. https://doi.org/10.1073/pnas.93.8.3497.
11. Franke-Fayard B, Janse CJ, Cunha-Rodrigues M, Ramesar J, Büscher P, Que I, Löwik C, Voshol PJ, den Boer MAM, van Duinen SG, Febbraio M, Mota MM, Waters AP. 2005. Murine malaria parasite sequestration: CD36 is the major receptor, but cerebral pathology is unlinked to sequestration. Proc Natl Acad Sci U S A 102:11468–11473. https://doi.org/10.1073/pnas.0503386102.
12. Amante FH, Stanley AC, Randall LM, Zhou Y, Haque A, McSweeney K, Waters AP, Janse CJ, Good MF, Hill GR, Engwerda CR. 2007. A role for natural regulatory T cells in the pathogenesis of experimental cerebral malaria. Am J Pathol 171:548–559. https://doi.org/10.2353/ajpath.2007.061033.
13. Riley EM, Couper KN, Helmby H, Hafalla JCR, de Souza JB, Langhorne J, Jarra WB, Zavala F. 2010. Neuropathogenesis of human and murine malaria. Trends Parasitol 26:277–278. https://doi.org/10.1016/j.pt.2010.03.002.

14. Martins YC, de Carvalho LJM, Daniel-Ribeiro CT. 2009. Challenges in the determination of early predictors of cerebral malaria: lessons from the human disease and the experimental murine models. Neuroimmunomodulation 16:134–145. https://doi.org/10.1159/000180268.
15. Martins YC, Smith MJ, Pelajo-Machado M, Werneck GL, Lenzi HL, Daniel-Ribeiro CT, Carvalho LJDM. 2009. Characterization of cerebral malaria in the outbred swiss webster mouse infected by *Plasmodium berghei* ANKA. Int J Exp Pathol 90:119–130. https://doi.org/10.1111/j.1365-2613.2008.00622.x.
16. Strangward P, Haley MJ, Shaw TN, Schwartz JM, Greig R, Mironov A, de Souza JB, Cruickshank SM, Craig AG, Milner DA, Allan SM, Couper KN. 2017. A quantitative brain map of experimental cerebral malaria pathology. PLoS Pathog 13:e1006267. https://doi.org/10.1371/journal.ppat.1006267.
17. Brian de Souza J, Riley EM. 2002. Cerebral malaria: the contribution of studies in animal models to our understanding of immunopathogenesis. Microbes Infect 4:291–300. https://doi.org/10.1016/S1286-4579(02)01541-1.
18. Penet M-F, Viola A, Confort-Gouny S, Fur Y, Duhamel G, Kober F, Ibarrola D, Izquierdo M, Coltel N, Gharib B, Grau GE, Cozzone PJ. 2005. Imaging experimental cerebral malaria *in vivo*: significant role of ischemic brain edema. J Neurosci 25:7352–7358. https://doi.org/10.1523/JNEUROSCI.1002-05.2005.
19. Ghosh S, Sengupta A, Sharma S, Sonawat HM. 2012. Metabolic fingerprints of serum, brain, and liver are distinct for mice with cerebral and noncerebral malaria: a 1H NMR spectroscopy-based metabonomic study. J Proteome Res 11:4992–5004. https://doi.org/10.1021/pr300562m.
20. Looareesuwan S, White NJ, Chanthavanich P, Juel-Jensen BE, Warrell DA, Sutharasamai P, Sundaravej K, Bunnag D, Harinasuta T. 1983. Do patients with cerebral malaria have cerebral oedema? a computed tomography study. Lancet 1:434–437. https://doi.org/10.1016/S0140-6736(83)91437-X.
21. Brown H, Hien TT, Day N, Mai NT, Chuong LV, Chau TT, Loc PP, Phu NH, Bethell D, Farrar J, Gatter K, White N, Turner G. 1999. Evidence of blood-brain barrier dysfunction in human cerebral malaria. Neuropathol Appl Neurobiol 25:331–340. https://doi.org/10.1046/j.1365-2990.1999.00188.x.
22. Thumwood CM, Hunt NH, Clark IA, Cowden WB. 1988. Breakdown of the blood-brain barrier in murine cerebral malaria. Parasitology 96:579–589. https://doi.org/10.1017/S0031182000080203.
23. Chan-Ling T, Neill AL, Hunt NH. 1992. Early microvascular changes in murine cerebral malaria detected in retinal wholemounts. Am J Pathol 140:1121–1130.
24. Potter S, Chan-Ling T, Ball HJ, Mansour H, Mitchell A, Maluish L, Hunt NH. 2006. Perforin mediated apoptosis of cerebral microvascular endothelial cells during experimental cerebral malaria. Int J Parasitol 36:485–496. https://doi.org/10.1016/j.ijpara.2005.12.005.
25. Chang WL, Jones SP, Lefer DJ, Welbourne T, Sun G, Yin L, Suzuki H, Huang J, Granger DN, Van der Heyde HC. 2001. $CD8^+$-T-cell depletion ameliorates circulatory shock in *Plasmodium berghei*-infected mice. Infect Immun 69:7341–7348. https://doi.org/10.1128/IAI.69.12.7341-7348.2001.
26. Belnoue E, Kayibanda M, Vigario AM, Deschemin J-C, van Rooijen N, Viguier M, Snounou G, Rénia L. 2002. On the pathogenic role of brain-sequestered $\alpha\beta$ $CD8^+$ T cells in experimental cerebral malaria. J Immunol 169:6369–6375. https://doi.org/10.4049/jimmunol.169.11.6369.
27. Barrera V, Haley MJ, Strangward P, Attree E, Kamiza S, Seydel KB, Taylor TE, Milner DA, Craig AG, Couper KN. 2019. Comparison of CD8+ T cell accumulation in the brain during human and murine cerebral malaria. Front Immunol 10:1747. https://doi.org/10.3389/fimmu.2019.01747.
28. Riggle BA, Manglani M, Maric D, Johnson KR, Lee MH, Abath Neto OL, Taylor TE, Seydel KB, Nath A, Miller LH, McGavern DB, Pierce SK. 2020. $CD8^+$ T cells target cerebrovasculature in children with cerebral malaria. J Clin Invest 130:1128–1138. https://doi.org/10.1172/JCI133474.
29. Rodrigues Goulart H, Kimura EA, Peres VJ, Couto AS, Aquino Duarte FA, Katzin AM. 2004. Terpenes arrest parasite development and inhibit biosynthesis of isoprenoids in plasmodium falciparum. Antimicrob Agents Chemother 48:2502–2509. https://doi.org/10.1128/AAC.48.7.2502-2509.2004.
30. Saito AY, Marin Rodriguez AA, Menchaca Vega DS, Sussmann RAC, Kimura EA, Katzin AM. 2016. Antimalarial activity of the terpene nerolidol. Int J Antimicrob Agents 48:641–646. https://doi.org/10.1016/j.ijantimicag.2016.08.017.
31. Rodriguez AAM, Carvalho LJM, Kimura EA, Katzin AM. 2018. Perillyl alcohol exhibits *in vitro* inhibitory activity against *Plasmodium falciparum* and protects against experimental cerebral malaria. Int J Antimicrob Agents 51:370–377. https://doi.org/10.1016/j.ijantimicag.2017.08.025.
32. Chen TC, Da Fonseca CO, Schönthal AH. 2015. Preclinical development and clinical use of perillyl alcohol for chemoprevention and cancer therapy. Am J Cancer Res 5:1580–1593.
33. Dondorp AM, Desakorn V, Pongtavornpinyo W, Sahassananda D, Silamut K, Chotivanich K, Newton PN, Pitisuttithum P, Smithyman AM, White NJ, Day NPJ. 2005. Estimation of the total parasite biomass in acute falciparum malaria from plasma. PLoS Med 2:e204. https://doi.org/10.1371/journal.pmed.0020204.
34. Ripple GH, Gould MN, Arzoomanian RZ, Alberti D, Feierabend C, Simon K, Binger K, Tutsch KD, Pomplun M, Wahamaki A, Marnocha R, Wilding G, Bailey HH. 2000. Phase I clinical and pharmacokinetic study of perillyl alcohol administered four times a day. Clin Cancer Rese 6:390–396.
35. Hudes GR, Szarka CE, Adams A, Ranganathan S, McCauley RA, Weiner LM, Langer CJ, Litwin S, Yeslow G, Halberr T, Qian M, Gallo JM. 2000. Phase I pharmacokinetic trial of perillyl alcohol (NSC 641066) in patients with refractory solid malignancies. Clin Cancer Rese 6:3071–3080.
36. Morgan-Meadows S, Dubey S, Gould M, Tutsch K, Marnocha R, Arzoomanin R, Alberti D, Binger K, Feierabend C, Volkman J, Ellingen S, Black S, Pomplun M, Wilding G, Bailey H. 2003. Phase I trial of perillyl alcohol administered four times daily continuously. Cancer Chemother Pharmacol 52:361–366. https://doi.org/10.1007/s00280-003-0684-y.
37. da Fonseca CO, Schwartsmann G, Fischer J, Nagel J, Futuro D, Quirico-Santos T, Gattass CR. 2008. Preliminary results from a phase I/II study of perillyl alcohol intranasal administration in adults with recurrent malignant gliomas. Surg Neurol 70:259–266. https://doi.org/10.1016/j.surneu.2007.07.040.
38. Pais TF, Penha-Gonçalves C. 2019. Brain endothelium: the "innate immunity response hypothesis" in cerebral malaria pathogenesis. Front Immunol 9:3100. https://doi.org/10.3389/fimmu.2018.03100.
39. Newbold C, Craig A, Kyes S, Rowe A, Fernandez-Reyes D, Fagan T. 1999. Cytoadherence, pathogenesis and the infected red cell surface in *Plasmodium falciparum*. Int J Parasitol 29:927–937. https://doi.org/10.1016/s0020-7519(99)00049-1.
40. Turner GDH, Morrison H, Jones M, Davis TME, Looareesuwan S, Buley ID, Gatter KC, Newbold C, Pukritayakamee S, Nagachinta B, White NJ, Berendt AR. 1994. An immunohistochemical study of the pathology of fatal malaria evidence for widespread endothelial activation and a potential role for intercellular adhesion molecule-1 in cerebral sequestration. Am J Pathol 145:1057–1069.
41. Shabani E, Hanisch B, Opoka RO, Lavstsen T, John CC. 2017. *Plasmodium falciparum* EPCR-binding PfEMP1 expression increases with malaria disease severity and is elevated in retinopathy negative cerebral malaria. BMC Med 15:1–14. https://doi.org/10.1186/s12916-017-0945-y.
42. Kessler A, Dankwa S, Bernabeu M, Harawa V, Danziger SA, Duffy F, Kampondeni SD, Potchen MJ, Dambrauskas N, Vigdorovich V, Oliver BG, Hochman SE, Mowrey WB, MacCormick IJC, Mandala WL, Rogerson SJ, Sather DN, Aitchison JD, Taylor TE, Seydel KB, Smith JD, Kim K. 2017. Linking EPCR-binding PfEMP1 to brain swelling in pediatric cerebral malaria. Cell Host Microbe 22:601–614. https://doi.org/10.1016/j.chom.2017.09.009.
43. Favre N, Da Laperousaz C, Ryffel B, Weiss NA, Imhof BA, Rudin W, Lucas R, Piguet PF. 1999. Role of ICAM-1 (CD54) in the development. Microbes Infect 1:961–968. https://doi.org/10.1016/S1286-4579(99)80513-9.
44. Cabrales P, Zanini GM, Meays D, Frangos JA, Carvalho LJM. 2011. Nitric oxide protection against murine cerebral malaria is associated with improved cerebral microcirculatory physiology. J Infect Dis 203:1454–1463. https://doi.org/10.1093/infdis/jir058.
45. Zanini GM, Cabrales P, Barkho W, Frangos JA, Carvalho LJM. 2011. Exogenous nitric oxide decreases brain vascular inflammation, leakage and venular resistance during *Plasmodium berghei* ANKA infection in mice. J Neuroinflammation 8:66. https://doi.org/10.1186/1742-2094-8-66.
46. Sierro F, Grau GER. 2019. The ins and outs of cerebral malaria pathogenesis: immunopathology, extracellular vesicles, immunometabolism, and trained immunity. Front Immunol 10:830. https://doi.org/10.3389/fimmu.2019.00830.
47. Curfs JH, Schetters TP, Hermsen CC, Jerusalem CR, van Zon AA, Eling WM. 1989. Immunological aspects of cerebral lesions in murine malaria. Clin Exp Immunol 75:136–140.
48. Imamura M, Sasaki O, Okunishi K, Nakagome K, Harada H, Kawahata K, Tanaka R, Yamamoto K, Dohi M. 2014. Perillyl alcohol suppresses antigen-induced immune responses in the lung. Biochem Biophys Res Commun 443:266–271. https://doi.org/10.1016/j.bbrc.2013.11.106.

49. d'Alessio PA, Mirshahi M, Bisson J, Béné MC. 2014. Skin repair properties of D-limonene and perillyl alcohol in murine models. AIAAMC 13:29–35. https://doi.org/10.2174/18715230113126660021.
50. Yeruva L, Pierre KJ, Elegbede A, Wang RC, Carper SW. 2007. Perillyl alcohol and perillic acid induced cell cycle arrest and apoptosis in non small cell lung cancer cells. Cancer Lett 257:216–226. https://doi.org/10.1016/j.canlet.2007.07.020.
51. Afshordel S, Kern B, Clasohm J, König H, Priester M, Weissenberger J, Kögel D, Eckert GP. 2015. Lovastatin and perillyl alcohol inhibit glioma cell invasion, migration, and proliferation–impact of Ras-/Rho-prenylation. Pharmacol Res 91:69–77. https://doi.org/10.1016/j.phrs.2014.11.006.
52. Gelb MH, Tamanoi F, Yokoyama K, Ghomashchi F, Esson K, Gould MN. 1995. The inhibition of protein prenyltransferases by oxygenated metabolites of limonene and perillyl alcohol. Cancer Lett 91:169–175. https://doi.org/10.1016/0304-3835(95)03747-k.
53. da Fonseca CO, Linden R, Futuro D, Gattass CR, Quirico-Santos T. 2008. Ras pathway activation in gliomas: a strategic target for intranasal administration of perillyl alcohol. Arch Immunol Ther Exp (Warsz) 56:267–276. https://doi.org/10.1007/s00005-008-0027-0.
54. Crowell PL, Chang RR, Ren Z, Elson CE, Gould MN. 1991. Selective inhibition of isoprenylation of 21–26-kDa proteins by the anticarcinogen d-limonene and its metabolites. J Biol Chem 266:17679–17685. https://doi.org/10.1016/S0021-9258(19)47425-5.
55. Wennerberg K, Rossman KL, Der CJ. 2005. The Ras superfamily at a glance. J Cell Sci 118:843–846. https://doi.org/10.1242/jcs.01660.
56. Carroll RW, Wainwright MS, Kim K-Y, Kidambi T, Gómez ND, Taylor T, Haldar K. 2010. A rapid murine coma and behavior scale for quantitative assessment of murine cerebral malaria. PLoS One 5:e13124-12. https://doi.org/10.1371/journal.pone.0013124.
57. Saito AY, Sussmann RAC, Kimura EA, Cassera MB, Katzin AM. 2015. Quantification of nerolidol in mouse plasma using gas chromatography–mass spectrometry. J Pharm Biomed Anal 111:100–103. https://doi.org/10.1016/j.jpba.2015.03.030.
58. Livak KJ, Schmittgen TD. 2001. Analysis of relative gene expression data using real-time quantitative PCR and the $2-\Delta\Delta CT$ method. Methods 25:402–408. https://doi.org/10.1006/meth.2001.1262.
59. Lee JJ, Cook M, Mihm MC, Xu S, Zhan Q, Wang J, Murphy GF, Lian CG. 2015. Loss of the epigenetic mark, 5-hydroxymethylcytosine, correlates with small cell/nevoid subpopulations and assists in microstaging of human melanoma. Oncotarget 6:37995–38004. https://doi.org/10.18632/oncotarget.6062.
60. Sawant S, Gokulan R, Dongre H, Vaidya M, Chaukar D, Prabhash K, Ingle A, Joshi S, Dange P, Joshi S, Singh AK, Makani V, Sharma S, Jeyaram A, Kane S, D'Cruz A. 2016. Prognostic role of Oct4, CD44 and c-Myc in radio–chemo-resistant oral cancer patients and their tumourigenic potential in immunodeficient mice. Clin Oral Invest 20:43–56. https://doi.org/10.1007/s00784-015-1476-6.
61. Alrashdan MS, Angel C, Cirillo N, McCullough M. 2016. Smoking habits and clinical patterns can alter the inflammatory infiltrate in oral lichenoid lesions. Oral Pathol Oral Radiol 121:49–57. https://doi.org/10.1016/j.oooo.2015.08.020.
62. Mane DR, Kale AD, Belaldavar C. 2017. Validation of immunoexpression of tenascin-C in oral precancerous and cancerous tissues using ImageJ analysis with novel immunohistochemistry profiler plugin: an immunohistochemical quantitative analysis. J Oral Maxillofac Pathol 21:211–217. https://doi.org/10.4103/jomfp.JOMFP_234_16.
63. Zanotto-Filho A, Rajamanickam S, Loranc E, Masamsetti VP, Gorthi A, Carolina J, Tonapi S, Mayer R, Reddick RL, Benavides R, Kuhn J, Chen Y, Bishop AJR. 2018. Sorafenib improves alkylating therapy by blocking induced inflammation, invasion and angiogenesis in breast cancer cells. Cancer Lett 425:101–115. https://doi.org/10.1016/j.canlet.2018.03.037.
64. Varghese F, Bukhari AB, Malhotra R, De A. 2014. IHC Profiler: an open source plugin for the quantitative evaluation and automated scoring of immunohistochemistry images of human tissue samples. PLoS One 9:e96801. https://doi.org/10.1371/journal.pone.0096801.
65. Rasband WS. 1997. ImageJ. U.S. National Institutes of Health, Bethesda, Maryland.